








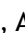

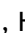






ORIGINAL

Medical Images Noise Removal using Improved Adversarial Generative Network

Eliminación de ruido en imágenes médicas mediante una red generativa adversarial

Ahmed A.F Osman¹  , Asma Abdulmana Alhamadi²  , Sultan Ahmad^{3,4}  , Rajit Nair⁵  , Mosleh Hmoud Al-Adhaileh⁶  , Ala Abdullah¹  , Hikmat A. M. Abdeljaber⁷  , Mohammed Ataelfadiel¹  

¹Applied College, King Faisal University. Al-Ahsa, 31982, Saudi Arabia.

²Department of Humanities, College of Science & Theoretical Studies, Saudi Electronic University. Riyadh, Saudi Arabia.

³Department of Computer Science, College of Computer Engineering and Sciences, Prince Sattam Bin Abdulaziz University. P.O.Box. 151, Alkharj 11942, Saudi Arabia.

⁴School of Computer Science and Engineering, Lovely Professional University. Phagwara, 144411, Punjab, India.

⁵VIT Bhopal University. Bhopal, India.

⁶Deanship of E-Learning and information technology, King Faisal University. Al-Ahsa 31982, Saudi Arabia.

⁷Department of Computer Science, Faculty of Information Technology, Applied Science Private University. Amman, Jordan.

Cite as: Osman AA, Alhamadi AA, Ahmad S, Nair R, Al-Adhaileh MH, Abdullah A, et al. Medical Images Noise Removal using Improved Adversarial Generative Network. *Seminars in Medical Writing and Education*. 2025; 4:838. <https://doi.org/10.56294/mw2025838>

Submitted: 18-03-2025

Revised: 04-07-2025

Accepted: 17-10-2025

Published: 18-10-2025

Editor: PhD. Prof. Estela Morales Peralta 

Corresponding Author: Sultan Ahmad 

ABSTRACT

Introduction: the protection of patient privacy through medical image de-identification stands as a vital yet complicated healthcare challenge which demands both accurate diagnosis and privacy protection. Deep learning techniques now provide superior methods to enhance medical images which suffer from acquisition noise and low-resolution degradation. The research develops a Generative Adversarial Network (GAN) architecture to create a deep-learning solution which enhances medical images while removing identifying information.

Objective: the proposed method uses adversarial learning to eliminate noise while restoring detailed high-resolution content from low-quality medical images.

Method: the research team analysed medical images through data analysis of their dataset. The GAN model received training and validation through experiments that compared its performance against established denoising and super-resolution techniques to assess its overall performance. The fundamental technology shows promise for future medical applications because it can enhance image quality to diagnose and treat multiple diseases. Medical image analysis requires images with diverse detailed features for proper evaluation.

Results: the proposed model demonstrates successful background noise reduction and improved image clarity with preserved diagnostic elements according to the obtained results. The proposed method achieved better results in PSNR and SSIM metrics than baseline models which proved its ability to restore vital diagnostic details.

Conclusions: the research introduces an innovative GAN-based system which delivers superior medical image quality while maintaining patient information confidentiality during de-identification processes. The method shows promise to create efficient and economical diagnostic processes through its ability to analyze poor-quality medical images.

Keywords: Computed Tomography; Magnetic Resonance; Noise Removal; Convolution Neural Networks; Adversarial Generative Network.

RESUMEN

Introducción: la protección de la privacidad del paciente mediante la desidentificación de imágenes médicas representa un desafío vital, aunque complejo, en la atención médica, que exige tanto un diagnóstico preciso como la protección de la privacidad. Las técnicas de aprendizaje profundo ofrecen ahora métodos superiores para mejorar las imágenes médicas que sufren ruido de adquisición y degradación por baja resolución. La investigación desarrolla una arquitectura de Red Generativa Antagónica (GAN) para crear una solución de aprendizaje profundo que mejora las imágenes médicas a la vez que elimina la información de identificación.

Objetivo: el método propuesto utiliza el aprendizaje antagónico para eliminar el ruido y restaurar el contenido detallado de alta resolución de imágenes médicas de baja calidad.

Método: el equipo de investigación analizó imágenes médicas mediante el análisis de datos de su conjunto de datos. El modelo GAN se entrenó y validó mediante experimentos que compararon su rendimiento con técnicas de demostración de eliminación de ruido y superresolución establecidas para evaluar su rendimiento general. Esta tecnología fundamental es prometedora para futuras aplicaciones médicas, ya que puede mejorar la calidad de la imagen para diagnosticar y tratar múltiples enfermedades. El análisis de imágenes médicas requiere imágenes con diversas características detalladas para una evaluación adecuada.

Resultados: el modelo propuesto demuestra una reducción eficaz del ruido de fondo y una mayor claridad de imagen, conservando los elementos diagnósticos, según los resultados obtenidos. El método propuesto obtuvo mejores resultados en las métricas PSNR y SSIM que los modelos de referencia, lo que demostró su capacidad para restaurar detalles diagnósticos vitales.

Conclusiones: la investigación presenta un innovador sistema basado en GAN que ofrece una calidad superior de imagen médica, manteniendo la confidencialidad de la información del paciente durante los procesos de desidentificación. El método promete crear procesos diagnósticos eficientes y económicos gracias a su capacidad para analizar imágenes médicas de baja calidad.

Palabras clave: Tomografía Computarizada; Resonancia Magnética; Eliminación de Ruido; Redes Neuronales Convolucionales; Red Generativa Adversarial.

INTRODUCTION

The increasing need for high-quality images in medical imaging and digital photography makes noise reduction techniques essential for achieving optimal results. The application of Improved Generative Adversarial Networks (GANs) in this field produces clearer images while maintaining critical details which standard filtering techniques tend to discard. The development of Wasserstein GANs (WGAN) and related variations in GAN architecture has proven to outperform traditional methods in denoising applications.⁽¹⁾ The ongoing research into GAN hyperparameter optimization and noise-specific GAN adaptations will enhance their performance which will result in major advancements for both immediate use cases and critical situations that require absolute precision.⁽²⁾

Denoising is a typical computer vision processing technique, this method can be used to restore polluted photos by removing noise created during the altering process. Denoising is an essential component of medical image processing because noise can obscure critical characteristics and influence clinical parameter selection.⁽³⁾ Denoising is necessary because noise can hide crucial information and delay diagnosis. PET gives metabolic and present strategy information, as opposed to computed tomography (CT) and magnetic resonance (MR), which provide high-resolution structural information.⁽⁴⁾ These modalities enable a variety of image collection methods to be used. To some extent, this is done to meet scan speed, radiation safety, and picture quality standards. CT scans have become significantly lower doses over the last decade as part of a push to safeguard patients from potentially hazardous levels of radiation.⁽⁵⁾ Even though there is no radiation risk, those with claustrophobia or other anxiety difficulties may struggle to relax during an MR scan. This is true even if radiation exposure is completely safe. Under-sampling k-space has been attempted to enhance efficiency, alleviate patient discomfort, and speed up MR scanning.⁽⁶⁾ One of the unique features of PET scanning is the process of creating a flawless image from a disorganized sequence of events.^(7,8) Image post-processing is straightforward to incorporate into existing healthcare practices and can be performed on damaged photographs right away. It is possible to use image post-processing on damaged photographs without jeopardizing current medical practices.

Several studies are currently being conducted to address problems that arise during the denoising of the original medical image. Common image processing methods used for medical image denoising include diffuse filters,⁽⁹⁾ column 3D,⁽¹⁰⁾ and anti-means.⁽¹¹⁾ While these methods can reduce noise to varying degrees, the results are typically excessively smooth and imprecise. This is because different approaches can reduce noise in different ways. Transfer learning, according to a recent study, outperforms alternative ways for executing several medical imaging-related duties. Categorization⁽¹²⁾, chemical breakdown⁽¹³⁾, and denoising⁽¹⁴⁾ are a few

examples. We referred to these CT readings several times throughout the investigation to reduce background CT noise. To restore under-sampled MR images⁽¹⁵⁾ employed denoising convolutional neural networks and k-space correction, a technique that employs a self-organizing adversarial network in the short run.⁽¹⁶⁾ The bulk of these methods have demonstrated success when applied to medical picture denoising tasks, and they accomplish this by designing case-dependent loss functions or optimizing network architecture. For specific cases, loss functions optimization of network architecture the content images, also known as full-dose or powerful images, can be learned directly or regressively extracted from the noise images. While noise learning can aid in the reduction of performance decreases while maintaining more topological and contrast information, content learning may result in more accurate noise cancellation.⁽¹⁷⁾

An encoder-decoder network that removes noise from confocal laser endomicroscopy images. To assist with this, priors generated from the noise and data were incorporated into the model. Learning the metal artifact as well as the content⁽¹⁸⁾ could lessen the occurrence of CT artifacts during network training. The goal is to limit the number of CT artifacts, new photos were taken with tainted metal artifact samples and the previously acquired artifact coding to illustrate consistent losses throughout cycles. Consider many alternatives for the medical picture diagnosis assignment that incorporate the best characteristics of the two instructional approaches. In the final subject prediction, both the content prior and the acoustic prior will be used more significantly. As a result, the suggested technique allows you to learn both the noise parts and the material at the same time.

Proposed Approach

the proposal provides a general-purpose denoising pipeline for medical images that makes use of the proposed technique as well as many deep, parallel convolution neural networks (CNNs) as predictors. This pipeline can help reduce noise in medical images. This pipeline, which focuses on the entire denoising process for medical images, was built using the GAN framework⁽¹⁷⁾ shown in figure 1. Four distinct sets of photos were used to evaluate how well the proposed technique worked. In comparison, the proposed strategy outperforms the most recent techniques. This is correct regardless of the evaluation criterion utilised. Finally, the proposed approach has been validated on many noisy datasets. The results show how robust our methodology is to various types of noise. The controllability of the method and its potential for widespread use is also carefully considered. It is vital to understand both the context and the topic matter when utilising the available resources. The illustration demonstrates the concept of using both the original and corrupted data sets to repair noisy photos (shown by the letters “corrupted” and “content”).⁽¹⁸⁾ As a result, there are two sets of similar images, one corrupted and one not (corrupted, unreadable, and obscure). The operation of computers will be taught with fictitious data, and the use of networking devices will be taught with fictitious static.

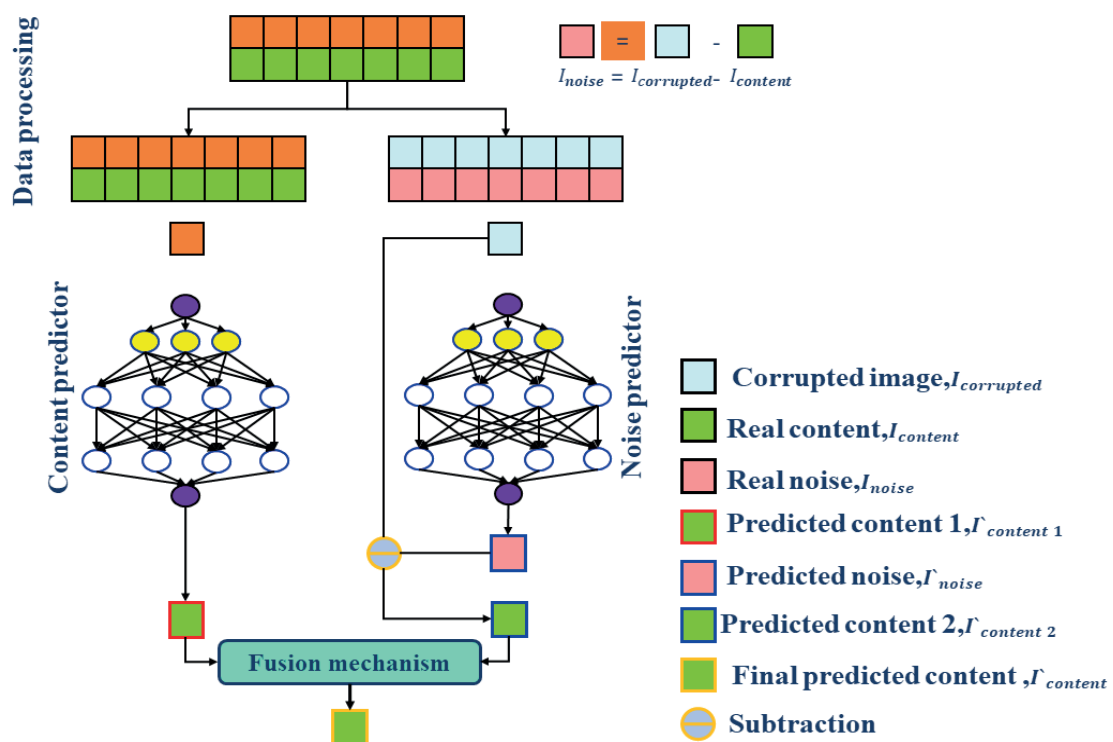


Figure 1. A Processing Pipeline to Denoise Medical Images

The administration of the SB is going well, the generative adversarial network (GAN) did an examination, and the proposed approach was used to improve the performance of the GAN system's component G, which oversaw transfer learning.⁽¹⁹⁾ The letter "G" in the acronym GAN is used throughout the structure to represent the word "generator." This is a conceivable negative outcome that could occur. According to previous studies,⁽²⁰⁾ using a discriminator improves how much the properties of denoised photos retain their original properties, this enhancement could be seen as a significant benefit. The GAN framework proposed is shown in figure 2 instead of using just one of the predictors, the generator employs both. This is because predictors and CNNs share the same network design, which explains why this is the case. Predictors and CNNs, for example, might be built using the same principles. The initial phase in the data fusion process is concatenating the data, and once that step is accomplished, the entire dataset is subjected to an order 1×1 convolution because convolution is already a process, the fusion process can be viewed as an extension of it because the weights can be taught, this will result in improved performance.

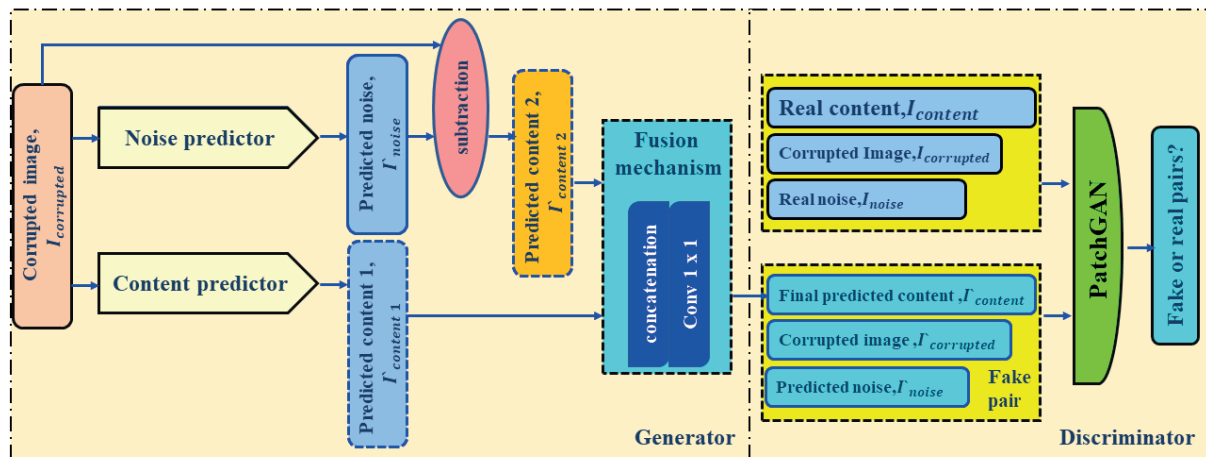


Figure 2. A Generative Adversarial Network-Based Proposed Method for Denoising Medical Images

This method is used to lessen the visibility of noise in digital photos, textural or stylistic information is lost when there is a structural mismatch in the size of the patches, which is a benefit of PatchGAN. PatchGAN is included as a classifier in the proposed GAN architecture because this is the case. The original picture pair ($I_{content}$, $I_{corrupted}$, or I_{noise}) can be given to the PatchGAN algorithm. The main goal of PatchGAN is to spot fake data and find real data. According to,⁽²¹⁾ the loss caused by PatchGAN is added to the loss caused by L1 to calculate our overall loss. DnCNN⁽²²⁾ and SRDenseNet⁽²³⁾ are two CNN models that are widely used and frequently represent the field. The essential features of the finished U-Net framework are depicted in figure 3a, which serves as an illustration for this inquiry. The original U-Net was improved in two ways: first, padding was added to ensure that the size was correct, and second, batch normalization⁽²⁴⁾ was added to provide regularization. Both changes were made to improve the U-Net. Regularization was identified as a possible area for advancement in each of these modifications. Figure 3b diagrammatically depicts the architecture of the DnCNN used in this work. This design was used in this study. In contrast to the DnCNN proposed in,⁽²⁵⁾ the one presented in this paper uses leaky ReLU in its computations rather than residual learning. This discrepancy is since⁽²⁶⁾ was written before the publication of this study. Figure 3d goes deeper into the dense block, whereas Figure 3c presents an overview of the SRDenseNet design at a high level. Figure 3 depicts both images. Both phone numbers are provided for your convenience. As a result, the layers that were causing the network to become unstable were eliminated. This was done to guarantee that the proportions of the finished image matched those of the original image used to train the network. This step was necessary to ensure that the finished image's dimensions matched those of the original.⁽²⁷⁾ We accomplished this by halving the number of convolutions in each dense block, which increased efficiency and allowed us to lower the total number of dense blocks from eight to six.

Some examples of acronyms are LR, which stands for Leaky ReLU; BN, which stands for batch normalization; and R, which stands for ReLU. We were able to successfully implement the proposed technique using a GAN; for the predictor part, we employed three regular CNNs. There are different names for the same idea, such as Leaky ReLU, Batch Normalization, and ReLU. During the second step of the data preparation technique, we employed four medical imaging datasets generated from CT, PET, and MR.⁽²⁷⁾ These datasets were used in the research. These investigations were conducted to provide additional evidence to support the proposed denoise strategy. In clinical practice, researchers often employ a wide range of accessible study methodologies. The term "low-dose imaging" encompasses both treatments. Figure 4 depicts the possibility of a wide range of

Dixon sequence. Each axial segment was photographed under four conditions: aqueous, fatty, in-phase, and contrasted. The created content pictures were employed in the process of making matching MR slices following full-sample MR slicing. The slices were then subjected to a three-dimensional Fourier transformation, which resulted in the creation of k-space. Using a four-fold mumbo jumbo under-sampling strategy, we were able to acquire access to the under-sampled K-space.⁽²⁹⁾ To recover the undersampled MR slices, a three-dimensional inverted fast Fourier series was used. Our current set of 6560 2D MR slices has 544384 usable pixels, bringing the total number of pixels to 544384. The MR data were examined using six different cross-validation approaches. For the sake of demonstration, assume that just two of the eight patients used during the training phase will be used again during the testing phase. It was discovered that the appropriate values for Moment 2 and Impulse 1 should be 0,5 and 0,999, respectively. Each cohort had two people in total, and the success rate was 0,0002 %. The priority ratio between 8 and 6 has changed, and it is now 100 for 8 and 1 accordingly. The design was developed based on studies on PatchGAN networks⁽³⁰⁾ and put through a series of tests to determine which denoising value is the most effective. Convolutional normalisation was performed using a normal distribution with a range of 0 to 0,02 and batch normalisation using a normal distribution with a range of 0 to 1 (1,0, 0,02). Before training began, both sets of weights and biases were reset to zero. Table I summarises the overall time spent training each of the 300 networks as well as the total number of training epochs.^(30,31) Figure 4 shows three types of medical imaging noise, as well as their corrupted (left) and uncorrupted (right) equivalents. The diagram displays these three types of noise (the middle and right columns). The CT, PET, MR, and MRI pictures are given in order of greatest to worst quality. CT data can be displayed in the value range. From the CT images of seven different patients, we generated 1,709 possible combinations of CT slices and 669 different pairs of CT slices.⁽³²⁾ These figures were derived from the images. PET scans were performed on 12 people with suspected brain endocrine tumors using three tesla-magnetized machines. Patients got PET scans 30 minutes after receiving an injection of 3,7 MBq/kg of an 18F-labeled tracer. After the raw data was processed, each PET scan received two independent reconstructions. The first reconstruction employed every piece of data, but the second reconstruction used only 10 % of the data. The acquisition and reconstruction matrices were set to 144 by 144, and 4,271 torso 2D PET slice pair acquisitions were completed. During each of the validation's five rounds, each 10-pair slice set was randomly assigned to either the training or test phase. In addition to the people in the PET dataset, eleven more people from the same clinical study were included.⁽³³⁾ This dataset collected information in the form of two-dimensional slices of the subjects' abdominal regions using MR. The scanner was used to collect both sets of data. To achieve three-dimensional operation, this system used the WFI strategy, commonly known as a two-point Dixon sequence. Each axial segment was photographed under four conditions: aqueous, fatty, in-phase, and contrasted. The created content pictures were employed in the process of making matching MR slices following full-sample MR slicing. The slices were then subjected to a three-dimensional Fourier transformation, which resulted in the creation of k-space. Using a four-fold mumbo jumbo under-sampling strategy, we were able to acquire access to the under-sampled K-space. To recover the under-sampled MR slices, a three-dimensional inverted fast Fourier series was used. Our current set of 6560 2D MR slices has 544384 usable pixels, bringing the total number of pixels to 544384. The MR data were examined using six different cross-validation approaches. For the sake of demonstration, assume that just two of the eight patients used during the training phase will be used again during the testing phase. Each network was trained on a Geforce RTX 2080Ti GPU using the PyTorch framework. Adam oversaw ensuring that each network had the best possible training. It was discovered that the appropriate values for Moment 2 and Impulse 1 should be 0,5 and 0,999, respectively. Each cohort had two people in total, and the success rate was 0,0002 %. The priority ratio between 8 and 6 has changed, and it is now 100 for 8 and 1 accordingly. The design was developed based on studies on PatchGAN networks and put through a series of tests to determine which denoising value is the most effective.⁽³⁴⁾ For convolutional normalisation, a normal distribution with a range of 0 to 0,02 was employed, but for batch normalization, a normal distribution with a range of 0 to 1 was utilised (1,0, 0,02). Before training began, both sets of weights and biases were reset to zero. Table 1 summarises the overall time spent training each of the 300 networks as well as the total number of training epochs.

Table 1. Summarises the Overall Time Spent Training Each of the 300 Networks as Well As The Total Number of Training Epochs

Datasets	Proposed Model-U-Net	Proposed Model-DnCNN	Proposed Model-SRDenseNet
CT dataset	42	36	32
PET dataset	28	24	22
MR dataset	95	85	70

Ablation Studies

The proposed technique was employed in the trials that were carried out, to do this, we exhaustively examined single-predictor analogues of proposed networks and their counterparts to compare them side by side. Proposed-U-Net was used to directly compare a content-only U-Net classifier to a noise-only U-Net prediction both comparisons relied on the same set of data to get their respective results. The goal was to create an environment in which each competitor could compete fairly. The table 2 below contains more information on the quantitative discoveries produced by the analytical investigations. These data indicate that the proposed approach should be used in some capacity. U-Net benefited the most from the proposed technique, more than DnCNN or SRDenseNet. Figure 5 depicts an example slice that was used in the ablation studies. In contrast to networks trained with a single predictor, this example shows that networks trained with the proposed approach produce denoised outputs with far lower residual noise.

The proposed approach deployment could be blamed for the unmanageable expansion of network parameters. We were able to more than double the number of parameters in the study by using proposed approach with two predictors. Furthermore, the system's usefulness might be demonstrated by comparing the proposed technique to only a restricted trailer predictor in the proposed method-U-Net. To address the larger representations required by the extended convolutional layers, our team constructed a wide U Net with more feature channels than the original version. In addition to the network design research, we investigated the feasibility of completely deleting the loss function. This was done in tandem with the network design study. PatchGAN inspired us to improve the initial loss function, and one of the adjustments we made was to provide a new L1 control parameter dubbed noisy. The significance of the additional L1 regularisation term of noise was determined by comparing two different proposed method-U-Nets using cross-entropy loss functions. A single proposed method-U-Net determined the overall loss using both factors. The study project's findings imply that including a regularisation term for noise can be extremely advantageous. The combination of the overall GAN loss, the L1 material losses, and the L1 disturbance losses significantly improved the denoising process's performance. As a result, both the content predictor and the sound predictor received increased attention during training, resulting in improved accuracy for both tasks. The supplemental information demonstrates how effectively the various noise removal methods perform on two typical CT slices with metastases, as illustrated in Figures 5 and 6. Low-contrast lesions, on the other hand, became less prominent, and denoised images revealed moderate stripe aberrations throughout. This idea can be supported by evidence. Although part of the original signal structure was preserved in the WGAN-VGG output, there was still a large amount of noise. The proposed method outperforms the analogous technique in terms of retaining more of the content in its original form and minimizing background noise. In other words, the proposed networks are more efficient. When compared to the other proposed networks presented, the proposed model-U-Net performed the best in terms of preserving the overall health of the vascular system. Table 3, which is provided below, lists the quantitative subsets of the entire test set that were considered. The numerical calculations supported the conclusions that might be inferred from our optical data.

Model	SSIM	RSME	PSNR(dB)
Proposed Model-U-Net	0,928±0,043	0,029±0,004	45,782± 2,664
U-Net	0,993±0,052	0,038±0,005	42,379± 2,780
one wide-U-Net	0,994±0,043	0,037±0,005	42,838± 2,698
Proposed Model-DnCNN	0,927±0,043	0,029±0,004	46,233± 2,655
DnCNN	0,922±0,043	0,032±0,004	44,609±2,234
Proposed Model-SRDenseNet	0,928 ±0,042	0,028±0,004	46,367 ± 2,629
SRDenseNet	0,922±0,043	0,032±0,004	44,660± 2,374

The reader can see the real image pair because it is displayed in the upper-left corner of the screen. When U-Net is used as a predictor, the ablation study can be found in the second and third columns. This is because these columns contain most of the results. Rows 4 and 5 reflect the results of a study conducted with the goal of eliminating DnCNN. The final two columns are devoted to ablation studies conducted with SRDenseNet. To obtain the picture of the noise, we begin with the image of the entire dose and subtract the image of the expected content from the image of the full dose. The range of values that can be displayed on the CT screen is between 160 and 240 HU.

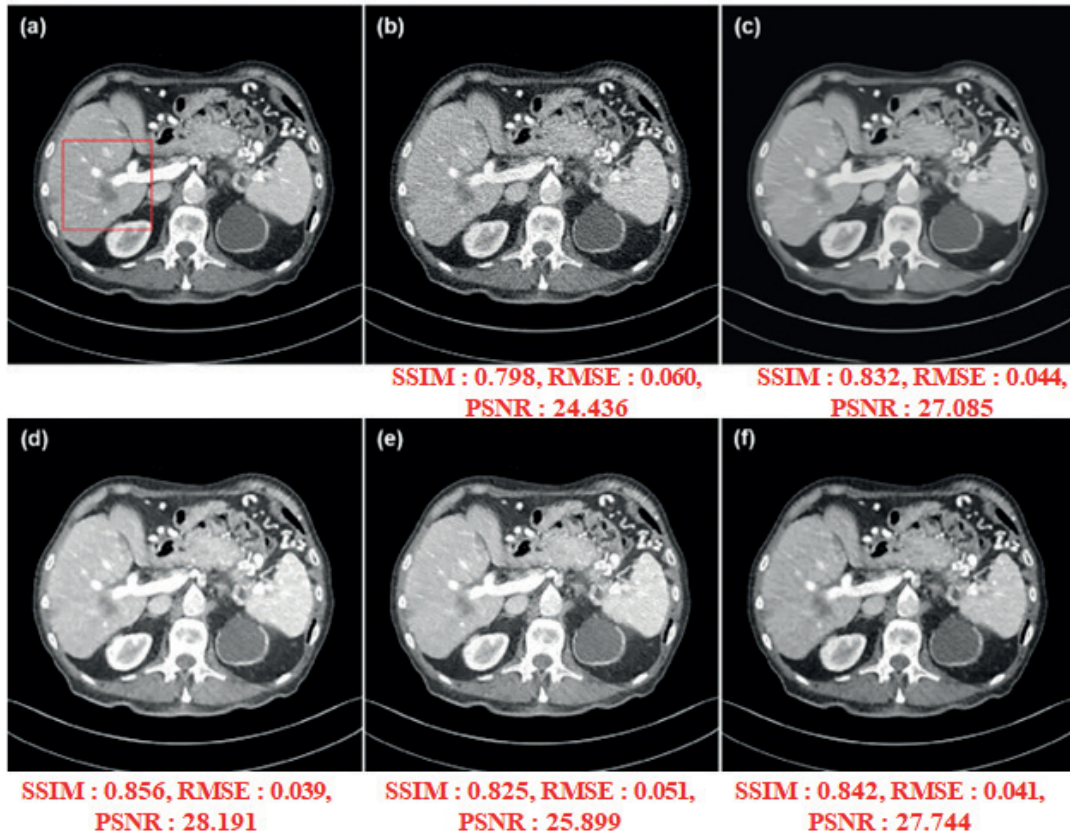


Figure 5. Maximum Dose of Computed Tomography (a) CT Dosage of 25 % (optional clause) (b) BM3D (b) RED-CNN (d) WGAN-VGG (e) Q-AE (f) Proposed model

	SSIM	RMSE	PSNR (dB)
45 % dose CT	0,952 ±0,074	0,044 ±0,009	39,993 ± 3,449
BM4D	0,998 ±0,042	0,036 ±0,004	42,989 ± 0,970
RED-CNN	0,922 ±0,043	0,035 ±0,009	43,934 ± 3,799
WGAN-VGG	0,996 ±0,052	0,039 ±0,022	42,623 ± 3,949
Q-AE	0,924 ±0,043	0,032 ±0,004	44,584 ± 2,692
Proposed Model-U-Net	0,928 ±0,043	0,029 ±0,004	45,782 ± 2,664
Proposed Model-DnCNN	0,927 ±0,043	0,029 ±0,004	46,233 ± 2,655
Proposed Model-SRDenseNet	0,928 ±0,042	0,028 ±0,004	46,367 ± 2,629

RESULTS

An examination of several methods for noise removal in CT Images of Poor-Quality thinking about a massive informational resource. Even though they were not initially recommended for use with the PET wavelet transform, the G SCAN, DnCNN, and cGAN algorithms were adapted and improved. We chose two slices with lesions, one coronal shown in figure 6 and one axial shown in figure 7 to conduct an objective visual evaluation of the performance of PET denoising. There were two extremely small lesions visible in the appropriate slices of the total number of images. Because they were focused on adjusting to the lower background noise levels, U-Net, DnCNN, and GAN failed to recognize the minute lesions. As a result, they were unable to focus on the image's features. The model was blurred to the point where a large amount of the finer texture of the original structure was destroyed. The proposed network that was presented could successfully conceal both background noise and underlying structural data. Table 4 contains further quantitative findings from the entire cross-validation procedure, as well as the means and standard deviations for each data set.

Table 4. Coronal Slice Mean and Standard Deviation Comparisons for Low-Dose PET Denoising Techniques			
	SSIM	RMSE	PSNR (dB)
30 % dose PET	0,982 ± 0,029	3,409 ± 2,227	52,885 ± 4,978
BM4D	0,987 ± 0,028	3,273 ± 0,925	52,939 ± 3,943
U-Net	0,984 ± 0,068	2,974 ± 2,099	54,399 ± 5,097
DnCNN	0,986 ± 0,026	3,266 ± 2,397	53,603 ± 5,020
GAN	0,990 ± 0,020	3,225 ± 2,295	53,862 ± 5,425
Proposed Model-U-Net	0,995 ± 0,020	2,897 ± 2,092	55,393 ± 5,557
Proposed Model-DnCNN	0,997 ± 0,009	2,846 ± 2,292	55,708 ± 5,527
Proposed Model-SRDenseNet	0,997 ± 0,009	2,869 ± 2,296	55,600 ± 5,577

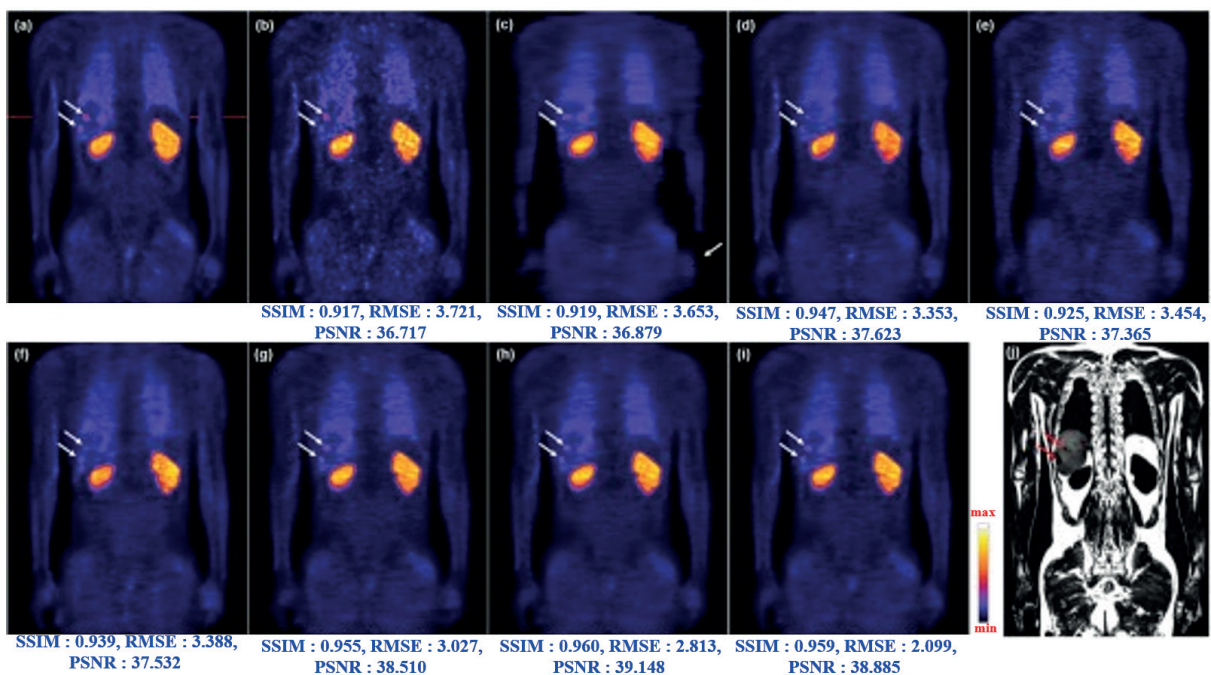


Figure 6. Low-dose PET noise reduction strategies compared along the coronal axis (a) A PET test is performed at the greatest dose allowable per protocol. in terms of dose (b) BM3D (c) 10 % PET (d) U-Net (e) DnCNN (f) GAN (g) The proposed model-U-Net (h) The proposed model-DnCNN (i) Proposed Model

The arrows indicate two little growths that can be noticed. because of these modifications, the networks' accuracy has improved. We extracted water and fat shots from the WFI sequences to evaluate the MR denoising objectively. Every deep learning-based system outperformed NLN when it came to removing noise from statistics, demonstrating that NLN is unsuitable for the task. SCNN, on the other hand, was used to scatter artefacts so that they could be found. The texture quality of U-Net and DnCNN has recently decreased dramatically. In terms of noise cancellation and structure restoration, the proposed network presented here outperform industry best practises. This finding could be influenced by the following factors: table 5 displays the final numerical results of the full cross-validation process. When compared to the approaches used as references, the proposed networks performed significantly better in every category.

To anticipate content and noise, the proposed networks did this to precisely forecast both the signal and the noise in the incoming data. Although proposed-S+D used two different CNN types, the findings obtained by both types on the presence of noise in the data were very comparable. Table 3 shows that proposed-DnCNN and proposed-SRDenseNet were both effective at lowering the RMSE and PSNR associated with low-dose CT denoising However, to achieve this augmentation, critical anatomical characteristics, such as the vessels seen in figure 5 by the red arrows, had to be concealed. proposed model -U-Net might be able to extract more information from the pixelated image. As a result, the distinction between blood vessels and lesions may be drawn more precisely. They all produced MR-dense images with acceptable overall visual quality. To maintain consistency, keep in mind that all three models were trained with the same set of inputs. Figure 8 depicts the numerical findings, whereas figure 8 depicts the process of selecting a sample slice for visual comparison. Both figures are contained in the same file. The two illustrations can be viewed together by viewing only one file.

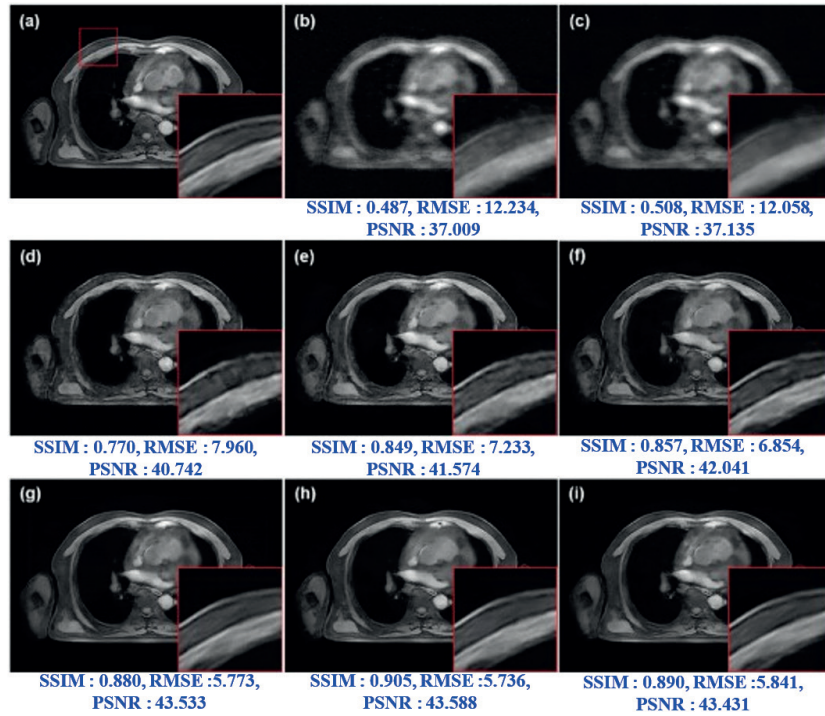


Figure 7. Different under-sampling (a) MR denoising algorithms work on WFI water images (b) MR for a four-to-one undersample (c) MR for a likelihood nearing its maximum value (d) SCNN (e) U-Net (f) DnCNN (g) DnCNN (h) SRDenseNet (i) Proposed Model

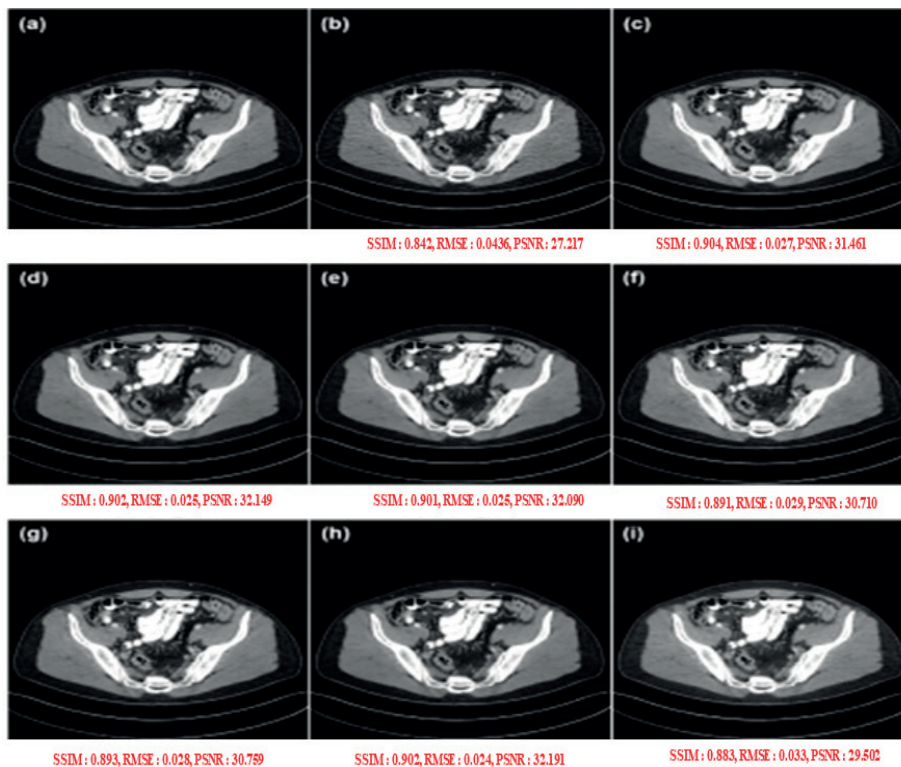


Figure 8. Quantitative Investigation of the noise-reduction capabilities of the CT dataset using the provided method's framework and a variety of various predictor possibilities (a) CT Dose of 25 Milligrams (b) Proposed model-Unet (c) Proposed model-DnCNN (d) Proposed model -SRDenseNet (e) Proposed model -U+D (f) Proposed model

Even though many CNN models work well for learning content, models with internal residual layers, like RDN and SRResNet, are probably not the best choice. This is due to the increased complexity of these models. The use of embedded residual layers improves the network's capacity to extract noise characteristics. When the label "content" was used, it's likely that the additional layers added an extra layer of complexity, making it harder to extract features that were relevant to the content. The DnCNN network was used to make noise, while the

SRDenseNet network was used to predict noise levels in a competitive way. This comparison was done to find out more about how well the proposed model works. Figure 8 depicts the qualitative findings, when it comes to precision and accuracy, the proposed model S+D is light years ahead of its predecessor. The DnCNN network was used to make noise, while the SRDenseNet network was used to predict noise levels in a competitive way. This comparison was done to find out more about how well the proposed model approach works. The proposed model S+D is light years ahead of its predecessor. The findings of the investigation revealed that the proposed model successfully taught both the noise and the content. We used the NIH-AAPM-Mayo CT datasets to train and test our method so we could see how well it worked in the WGAN-VGG architecture. We renamed the program's proposed model -WGAN-VGG to reflect the modifications we made to the proposed model component of the WGAN-VGG generator. One of these changes was the addition of a second CNN with the same design as the first. One CNN instructs another on data collection, and both CNNs are trained to detect background noise. Figure 9 shows how the WGAN-VGG and the proposed model-WGAN noise-reduction VGG compare in terms of their abilities. The quantity of residual noise in the proposed model-WGAN-VGG algorithm's results was greatly reduced. In all three categories, WGAN-performance VGGs performed worse than in previous years.

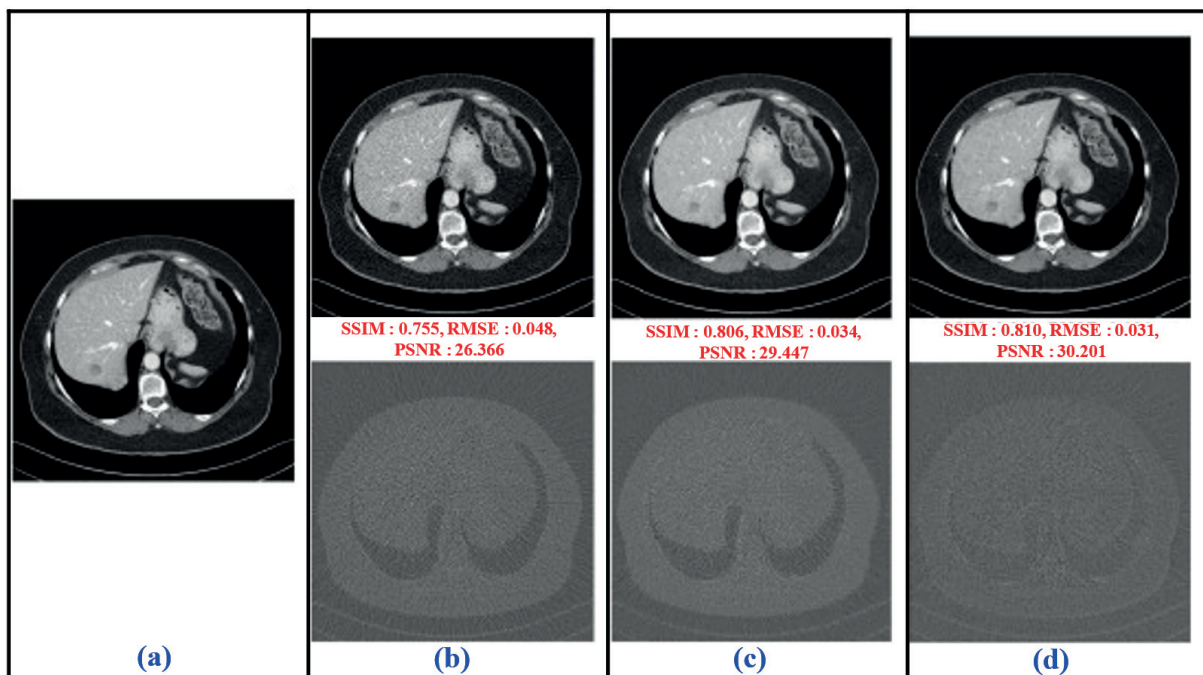


Figure 9. Utilizing computed tomography at the maximum effective dosage (a) The recommended dose of CT is 25 mg (optional clause). (b) The initial version of the WGAN-VGG (c) proposed model-WGAN-VGG (d) Proposed Model. The range of values that can be displayed on the CT screen is between 160 and 240 HU

We used the proposed method to develop a new loss function, and we confined its use to mean squared error to improve precision. The MR dataset was used consistently throughout the study project's training and testing phases. Figure 10 graphically depicts the numerical findings, which can be arranged in the following ways: the results clearly suggest that the proposed technique may be employed without the GAN framework. In addition to the GAN, the content provides indicators that can be used to employ a variety of other frameworks.

The third addition to the NID consists of the following components, which can be found in the following: We also investigated the ability to remove noise using a dataset called SIDD, which contains photographs taken under identical conditions as when they were first captured. SIDD was created by recording ten diverse instances with five different mobile phone types under varying lighting conditions. We also used these components. SIDD-Small is a scaled-down version of the full SIDD dataset that was used for this inquiry. There was a total of 1024 pictures taken from the SIDD-Small collection, each with paired dimensions of 256 pixels by 256 pixels. In addition to the 320 previously gathered training image pairs, we used a total of 704 test photo pairings to create our model. It includes some denoised versions of photos derived from the SIDD-Small dataset. These several versions were created because of a variety of strategies used during the development process. Table 5 lists the quantitative parameters that are considered while evaluating candidates for open positions. The conclusion we reached by visually examining the evidence was backed by numerical evidence.

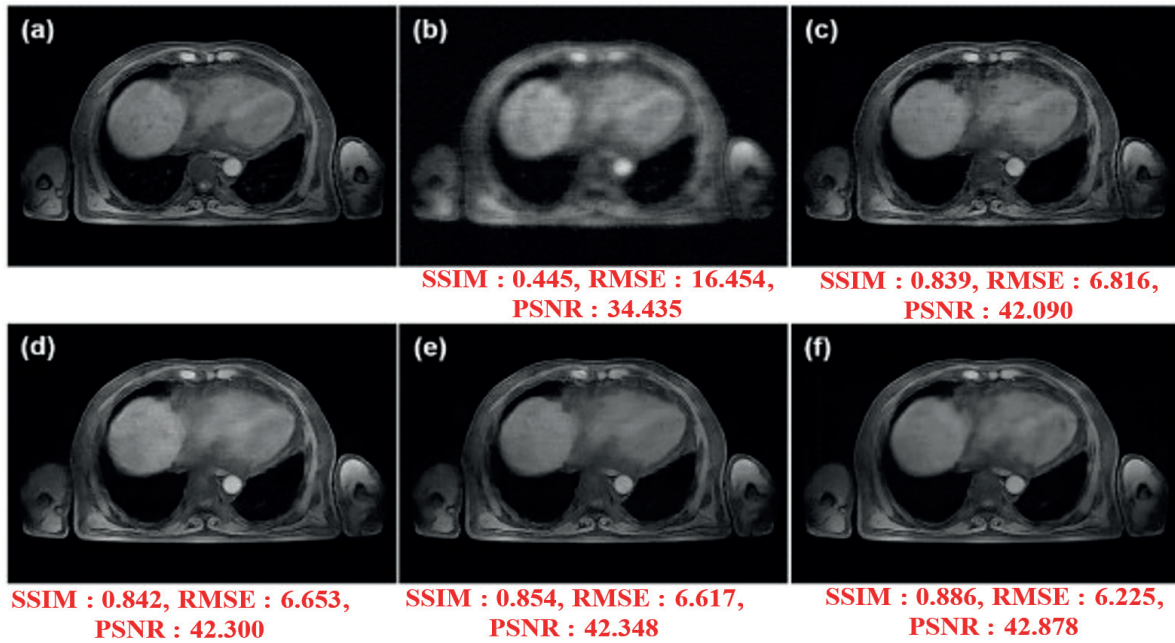


Figure 10. Comparison of Denoising Algorithms

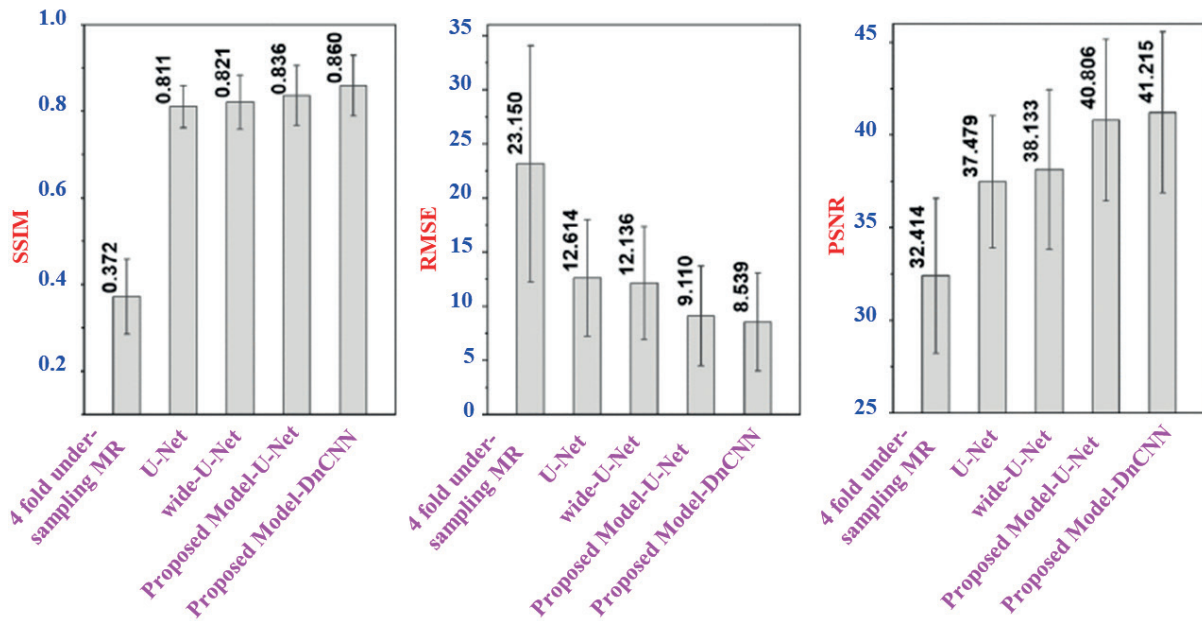


Figure 11. The Specific Data Extracted from The MR Dataset

	SSIM	RMSE	PSNR (dB)
Before denoising	0,547 ±0,279	23,973 ± 7,022	37,867 ± 4,786
BM4D	0,974 ±0,098	8,399 ± 4,724	42,998 ± 5,630
NLM	0,792 ± 0,292	8,999 ± 5,059	42,357 ± 5,399
U-Net	0,922 ±0,059	5,505 ±3,009	46,948±4,398
DnCNN	0,747 ±0,294	9,827 ±6,067	39,592±5,584
SRDenseNet	0,999 ±0,075	5,380 ±3,007	47,453±4,827
Tyan-Net	0,935 ±0,064	4,954 ±2,906	48,047±4,780
Proposed Model-U-Net	0,969 ±0,052	4,227 ±2,928	49,670±5,776
Proposed Model-DnCNN	0,939 ±0,060	4,909 ±2,923	48,555±4,979
Proposed Model-SRDenseNet	0,948 ±0,054	4,804 ±2,925	48,839±5,046

The distribution difference, often known as the domain shift conundrum, is an example of a problem that happens frequently in clinical practice. This difficulty is caused by the problem. To determine how well a deep learning model is performing, rigorous generalisation testing is required. We prepared and carried out two exploratory experiments in different domains to examine the degree of generalizability of the proposed model networks that we built. Real CT scan images of a dosing piglet at 100 % and 75 % magnification were used in the investigation. These photographs were used in two sizes: 100 % and 75 % of their original size. Other variations between the two data sets include the scanned object, tube output, and tube current, in addition to the scanner model. We investigated proposed model in connection to the NIH-AAPM-Mayo CT dataset since Q-AE performed the best overall. The appendices provide Table 6, which present quantitative and qualitative data, respectively. Both sets of information are provided below. When compared to Q-AE networks, proposed model had much less residual noise after processing.

	SSIM	RMSE	PSNR (dB)
Before denoising	0,949 ± 0,036	0,063 ± 0,020	36,865 ± 3,979
Q-AE	0,992 ± 0,065	0,056 ± 0,042	37,954 ± 4,255
Proposed Model-U-Net	0,947 ± 0,035	0,050 ± 0,029	38,894 ± 4,024
Proposed Model-DnCNN	0,938 ± 0,024	0,053 ± 0,042	38,899 ± 3,959
Proposed Model-SRDenseNet	0,942 ± 0,035	0,053 ± 0,026	38,787 ± 3,990

Using the proposed model-U-Net, we deidentified a set of prostate-specific MR images. The proposed model-U-Net was trained using an abdominal MR image dataset. This demonstrates that the proposed technique can be used with a wide variety of MR scans. The same PET/MR scanner that was used to gather data for the prostate MR investigation was used to collect data for the abdominal MR examination. This was done to ensure consistency. This precaution was taken to ensure that there would be no departures from the norm. T2WI was used to diagnose specific lesions, but WFI was used as the MR sequence for the prostate pictures in the training dataset. This was done to ensure the accuracy of the results. Figure 11 indicates that, despite the uneven distribution of the data, the prostate MR denoising validation was successful. The PSNR increased from 25,445 to 26,505 dB, the RMSE decreased from 41,955 dB, and the SSIM decreased from 0,405 dB after the proposed model-U-Net was applied to the whole prostate MR test set. The introduction of a denoising model resulted in a significant improvement not only in the recovery of structures within the MR images but also in the recovery of intensities. Because the combined PET imaging shows a decreased T2 signal in the right anterior region, cancer can be identified with certainty. Prior to the denoising method, MR was performed using a sample size that was four times smaller. After removing the background noise with the proposed model -U-Net a PET scan image was superimposed on an MR scan. These findings indicate that the established proposed model has a high degree of generalizability to “unseen” medical imaging, which bodes well for its prospective therapeutic application.

CONCLUSIONS

The research developed an adversarial generative network to enhance medical image denoising which resulted in better diagnostic image quality and protected patient information confidentiality. The main goal of this research focused on creating a denoising system which would learn both structural elements and noise characteristics to generate diagnostic-quality images. The research demonstrates medical image enhancement through GAN-based frameworks which use multiple convolutional predictors to achieve advanced adversarial learning across different imaging types. The research approach depends on deep generative models to achieve both image clarity and diagnostic reliability and data privacy protection instead of depending on numerical assessment methods. The study demonstrates how GAN-based denoising frameworks adjust to changing clinical demands and different imaging environments. The proposed model establishes a base system which researchers can use to develop real-time reconstruction methods and combine multiple data types and create low-dose imaging systems. The research demonstrates that enhanced adversarial generative networks will drive medical image analysis progress while protecting patient privacy in healthcare systems.

BIBLIOGRAPHIC REFERENCES

1. Li Z. Image denoising methods based on GANs. *Applied and Computational Engineering*. 2024;106(1):25-31.
2. Ghadekar P, Gundawar A, Kamnapure S, Manjramkar D, Gujarathi I, Deore D. Improving image quality of noisy images through denoising and Style GAN technique. 2023:1-6.

3. Mohd Sagheer SV, George SN. A review on medical image denoising algorithms. *Biomed Signal Process Control*. 2020;61.
4. Geng M, Meng X, Yu J, Zhu L, Jin L, Jiang Z, et al. Content-noise complementary learning for medical image denoising. *IEEE Trans Med Imaging*. 2022;41(2):407-19.
5. Nair R, Vishwakarma S, Soni M, Patel T, Joshi S. Detection of covid-19 cases through X-ray images using hybrid deep neural network. *World J Eng*. 2021;19(1):33-9.
6. Poonguzhali R, Ahmad S, Sivasankar PT, et al. Automated brain tumor diagnosis using deep residual u-net segmentation model. *Comput Mater Contin*. 2023;74(1):2179-94.
7. Donoho DL. Compressed sensing. *IEEE Trans Inf Theory*. 2006;52(4):1289-306.
8. Agbley BLY, Li JP, Haq AU, et al. Federated Fusion of Magnified Histopathological Images for Breast Tumor Classification in the Internet of Medical Things. *IEEE J Biomed Health Inform*. 2023.
9. Manjón JV, Carbonell-Caballero J, Lull JJ, García-Martí G, Martí-Bonmatí L, Robles M. MRI denoising using non-local means. *Med Image Anal*. 2008;12(4):514-23.
10. Feruglio PF, Vinegoni C, Gros J, Sbarbati A, Weissleder R. Block matching 3D random noise filtering for absorption optical projection tomography. *Phys Med Biol*. 2010;55(18):5401.
11. Mendrik AM, Vonken EJ, Rutten A, Vieregger MA, van Ginneken B. Noise reduction in computed tomography scans using 3-D anisotropic hybrid diffusion with continuous switch. *IEEE Trans Med Imaging*. 2009;28(10):1585-94.
12. Ronneberger O, Fischer P, Brox T. U-Net: Convolutional networks for biomedical image segmentation. In: *Proceedings of the International Conference on Medical Image Computing and Computer-Assisted Intervention*. 2015. p. 234-41.
13. Lu Y, et al. A learning-based material decomposition pipeline for multi-energy X-ray imaging. *Med Phys*. 2019;46(2):689-703.
14. Geng M, et al. PMS-GAN: Parallel multi-stream generative adversarial network for multi-material decomposition in spectral computed tomography. *IEEE Trans Med Imaging*. 2021;40(2):571-84.
15. Chen H, et al. Low-dose CT with a residual encoder-decoder convolutional neural network. *IEEE Trans Image Process*. 2017;36(12):2524-35.
16. Fan F, et al. Quadratic autoencoder (Q-AE) for low-dose CT denoising. *IEEE Trans Med Imaging*. 2020;39(6):2035-50.
17. Shan H, et al. 3-D convolutional encoder-decoder network for low-dose CT via transfer learning from a 2-D trained network. *IEEE Trans Med Imaging*. 2018;37(6):1522-34.
18. Yi X, Babyn P. Sharpness-aware low-dose CT denoising using conditional generative adversarial network. *J Digit Imaging*. 2018;31(5):655-69.
19. Nair R, Singh DK, Ashu, Yadav S, Bakshi S. Hand gesture recognition system for physically challenged people using IOT. In: *2020 6th International Conference on Advanced Computing and Communication Systems (ICACCS)*. 2020.
20. Kashyap R, Nair R, Gangadharan SM, Botto-Tobar M, Farooq S, Rizwan A. Glaucoma detection and classification using improved U-Net Deep Learning Model. *Healthcare*. 2022;10(12):2497.
21. Lee D, Yoo J, Ye JC. Deep artifact learning for compressed sensing and parallel MRI. *arXiv:1703.01120*. 2017.
22. Han Y, Yoo J, Kim HH, Shin HJ, Sung K, Ye JC. Deep learning with domain adaptation for accelerated projection-reconstruction MR. *Magn Reson Med*. 2018;80(3):1189-205.

23. Hyun CM, Kim HP, Lee SM, Lee S, Seo JK. Deep learning for undersampled MRI reconstruction. *Phys Med Biol.* 2018;63(13).
24. Jiang D, Dou W, Vosters L, Xu X, Sun Y, Tan T. Denoising of 3D magnetic resonance images with multi-channel residual learning of convolutional neural network. *Jpn J Radiol.* 2018;36(9):566-74.
25. Kidoh M, et al. Deep learning based noise reduction for brain mr imaging: Tests on phantoms and healthy volunteers. *Magn Reson Med Sci.* 2020;19(3):195.
26. Xiang L, et al. Deep auto-context convolutional neural networks for standard-dose PET image estimation from low-dose PET/MRI. *Neurocomputing.* 2017;267:406-16.
27. Sano A, Nishio T, Masuda T, Karasawa K. Denoising PET images for proton therapy using a residual U-Net. *Biomed Phys Eng Exp.* 2021;7(2).
28. Wang Y, et al. 3D conditional generative adversarial networks for high-quality PET image estimation at low dose. *NeuroImage.* 2018;174:550-62.
29. Zhang K, Zuo W, Chen Y, Meng D, Zhang L. Beyond a Gaussian Denoiser: Residual learning of deep CNN for image denoising. *IEEE Trans Image Process.* 2017;26(7):3142-55.
30. Tong T, Li G, Liu X, Gao Q. Image super-resolution using dense skip connections. In: *Proceedings of the IEEE International Conference on Computer Vision (ICCV).* 2017. p. 4799-807.
31. Isola P, Zhu JY, Zhou T, Efros AA. Image-to-image translation with conditional adversarial networks. In: *Proceedings of the IEEE Conference on Computer Vision and Pattern Recognition.* 2017. p. 1125-34.
32. Sun H, Peng L, Zhang H, He Y, Cao S, Lu L. Dynamic PET image denoising using deep image prior combined with regularization by denoising. *IEEE Access.* 2021;9:52378-92.
33. Haq AU, Li JP, Ahmad S, Khan S, Alshara MA, Alotaibi RM. Diagnostic approach for accurate diagnosis of COVID-19 employing deep learning and transfer learning techniques through chest X-ray images clinical data in E-healthcare. *Sensors.* 2021;21(24):8219.
34. Alharbi M, Ahmad S. Enhancing COVID-19 detection using CT-scan image analysis and disease classification: the DI-QL approach. *Health Technol.* 2025;15:477-88.

FUNDING

This work was supported by the Deanship of Scientific Research, Vice Presidency for Graduate Studies and Scientific Research, King Faisal University, Saudi Arabia (Grant No. KFU253486).

AVAILABILITY OF DATA AND MATERIALS

The datasets used in this research are publicly available and properly cited in our dataset section for transparency and ease of replication.

CONFLICT OF INTEREST

The authors declare that they have no known competing financial interests or personal relationships that could have appeared to influence the work reported in this paper.

AUTHORSHIP CONTRIBUTION

Conceptualization: Ahmed A.F Osman, Rajit Nair, Sultan Ahmad, Hikmat A. M. Abdeljaber, Mosleh Hmoud Al-Adhaileh, Mohammed Ataelfadiel.

Investigation: Ahmed A.F Osman, Sultan Ahmad, Asma Abdulmana Alhamadi, Mohammed Ataelfadiel.

Methodology: Sultan Ahmad, Rajit Nair, Ahmed A.F Osman, Hikmat A. M. Abdeljaber, Mosleh Hmoud Al-Adhaileh.

Writing - original draft: Ahmed A.F Osman, Rajit Nair, Sultan Ahmad, Mosleh Hmoud Al-Adhaileh, Hikmat A. M. Abdeljaber, Ala Abdullah, Mohammed Ataelfadiel.

Writing - review and editing: Sultan Ahmad, Rajit Nair, Asma Abdulmana Alhamadi, Hikmat A. M. Abdeljaber, Mosleh Hmoud Al-Adhaileh, Ala Abdullah.